remote sensing

MDPI

Article

Observations, Remote Sensing, and Model Simulation to Analyze Southern Brazil Antarctic Ozone Hole Influence

Lucas Vaz Peres [1,*], Damaris Kirsh Pinheiro [2], Hassan Bencherif [3], Nelson Begue [3], José Valentin Bageston [4], Gabriela Dorneles Bittencourt [4], Thierry Portafaix [3], Andre Passaglia Schuch [5], Vagner Anabor [2], Rodrigo da Silva [6], Theomar Trindade de Araujo Tiburtino Neves [1], Raphael Pablo Tapajós Silva [1], Gabriela Cacilda Godinho dos Reis [6], Marco Antônio Godinho dos Reis [2], Maria Paulete Pereira Martins [7], Mohamed Abdoulwahab Toihir [8], Nkanyiso Mbatha [9], Luiz Angelo Steffenel [10] and David Mendes [11]

1 Institute of Engineering and Geosciences, Federal University of Western Para (UFOPA), Santarem 68040-255, Brazil; theomar.neves@ufopa.edu.br (T.T.d.A.T.N.); raphael.silva@ufopa.edu.br (R.P.T.S.)
2 Graduate Program in Meteorology, Federal University of Santa Maria (UFSM), Santa Maria 97105-900, Brazil; damaris@ufsm.br (D.K.P.); vanabor@ufsm.br (V.A.); reis.marco@acad.ufsm.br (M.A.G.d.R.)
3 Laboratoire de l'Atmosphère et des Cyclones—LACy, Université de La Réunion, UMR 8105, 97744 Saint-Denis, France; hassan.bencherif@univ-reunion.fr (H.B.); nelson.begue@univ-reunion.fr (N.B.); thierry.portafaix@univ-reunion.fr (T.P.)
4 Southern Space Coordination, National Institute for Space Research, Santa Maria 97105-900, Brazil; jose.bageston@inpe.br (J.V.B.); gabriela.bittencourt@inpe.br (G.D.B.)
5 Post-Graduation Program in Biological Sciences—Toxicological Biochemistry, Federal University of Santa Maria (UFSM), Santa Maria 97105-900, Brazil; andre.schuch@ufsm.br
6 Post-Graduate Program in Nature, Development and Society, Federal University of Western Para (UFOPA), Santarem 68040-255, Brazil; rodrigo.silva@ufopa.edu.br (R.d.S.); gabriela.reis@discente.ufopa.edu.br (G.C.G.d.R.)
7 General Coordination of Engineering, Technology and Space Sciences, National Institute for Space Research, São José dos Campos 12227-010, Brazil; maria.paulete@inpe.br
8 Agence Nationale de l'Aviation Civile et de la Météorologie, Moroni 84646, Comoros
9 Department of Geography, University of Zululand, KwaDlangezwa, Empangeni 3886, South Africa; mbathanb@unizulu.ac.za
10 Laboratoire d'Informatique en Calcul Intensif et Image pour la Simulation—LICIIS, University of Reims Champagne-Ardenne, 51687 Reims, France; luiz-angelo.steffenel@univ-reims.fr
11 Post-Graduate Program in Climate Science, Federal University of Rio Grande do Norte, Natal 59078-970, Brazil; david.mendes@ufrn.br
* Correspondence: lucas.peres@ufopa.edu.br

check for updates

Citation: Peres, L.V.; Pinheiro, D.K.; Bencherif, H.; Begue, N.; Bageston, J.V.; Bittencourt, G.D.; Portafaix, T.; Schuch, A.P.; Anabor, V.; da Silva, R.; et al. Observations, Remote Sensing, and Model Simulation to Analyze Southern Brazil Antarctic Ozone Hole Influence. *Remote Sens.* **2024**, *16*, 2017. https://doi.org/10.3390/rs16112017

Academic Editors: Wuke Wang, Yang Gao, Jiali Luo and Manuel Antón

Received: 18 November 2023
Revised: 28 December 2023
Accepted: 4 January 2024
Published: 4 June 2024

Abstract: This paper presents the observational, remote sensing, and model simulation used to analyze southern Brazil Antarctic ozone hole influence (SBAOHI) events that occurred between 2005 and 2014. To analyze it, we use total ozone column (TOC) data provided by a Brewer spectrophotometer (BS) and the OMI (Ozone Monitoring Instrument). In addition to the AURA/MLS (Microwave Limb Sounder) instrument, satellite ozone profiles were utilized with DYBAL (Dynamical Barrier Localization) code in the MIMOSA (Modélisation Isentrope du Transport Mésoéchelle de l'Ozone Stratosphérique par Advection) model Potential Vorticity (PV) fields. TOC has 7.0 ± 2.9 DU reductions average in 62 events. October has more events (30.7%). Polar tongue events are 19.3% in total, being more frequently observed in October (50% of cases), with medium intensity (58.2%), and in the stratosphere medium levels (55.0%). Already, polar filament events (80.7%) are more frequent in September (32.0%), with medium intensity (42.0%), and stratosphere medium levels (40.7%).

Keywords: Antarctic; ozone; MIMOSA model

1. Introduction

Ozone transport in the stratosphere is an essential factor in defining the concentration of atmospheric trace constituents in particular regions around the globe [1,2], including

the higher polar ozone concentrations compared with more production in the equatorial region. However, the global-scale stratospheric Brewer–Dobson circulation transports ozone from the equatorial region to the polar region [3,4]. This stratospheric circulation is still frequently studied [5,6].

Stratospheric components such as water vapor, nitrous oxide, and ozone are studied using PV analysis [7]. The authors [8,9] first discussed the stratospheric isentropic surfaces. This variable is important to the dynamic tracing definition of air masses, behaving like a material surface that has potential temperature conservation [10]. Using PV as a horizontal coordinate [11], one can determine the stratospheric polar vortex (SPV) edge as the maximum gradient region, capturing the insulation distribution effects within the SPV [12,13]. Furthermore, meridional PV gradients and long-lived trace atmospheric gases reveal that isentropic horizontal exchanges between tropical and extra-tropical regions are controlled by stratospheric dynamic barriers [14,15].

The polar South Hemisphere springtime ozone reduction, called "Antarctic Ozone Hole (AOH)" [16–18], is caused by polar stratospheric vortex formation [19,20] and heterogenic reactions that occur on the surface of polar stratospheric clouds [21,22]. The ozone hole began to draw the attention of the scientific community, and many studies have been conducted since the 1980s through polar ozone observational data in the South Hemisphere [23–25], and since the 1990s in the same way, but with important differences in the dynamical processes that affect ozone destruction compared to the North Hemisphere [26–28].

Climate change may affect stratospheric dynamic and thermodynamic processes by increasing polar vortex strength, thereby increasing ozone depletion in polar regions [29]. This ozone may also be destroyed and/or produced due to solar variations [30] or influenced by the stratosphere temperature, which is highly influenced by winter air mass stability and its effects on the polar vortex [31]. Furthermore, there are recent indications of ozone hole area reductions throughout the last decade [32,33].

The mid-latitudes close to the polar regions may have their ozone content directly influenced by the passage of the edge of the polar vortice through these regions, reducing ozone and increasing ultraviolet radiation levels [34–37]. Polar vortex can be perturbed by planetary wave activity increasing and this contributes to polar vortex ejection, through polar filaments that move to middle latitudes [38]. Rossby wave breaking causes PV filaments events [11,39], carrying South Pole air masses into middle latitudes, indirectly influencing the TOC in these regions [40]. The polar air sources are largely dominated by stratosphere vortex excursions and filaments events [41].

The authors of [42] presented stratospheric ozone extreme anomalies observed in middle latitudes related to stratospheric meridional transport over regions. Polar filaments may be isolated for 7 to 20 days after polar vortex separation, and this may be sufficient for their lower and middle latitudes propagation, causing a temporary TOC reduction [43–45]. The local ozone profile measurement reveals particular anomalies or lamina when passing these filaments [46]. The global character of these stratospheric transports from polar regions toward middle latitudes in the South Hemisphere was registered in South America [35,47], South Africa [48], and New Zealand [49].

High-resolution transport models [50,51] or contour advection [52] can correctly depict the ozone reduction lamina observed. Moreover, [53], using a PV contour advection MIMOSA model (Modele Isentropique du transport Mesoechelle de l'Ozone Stratospherique par Advection) [54], analyzed an important middle and tropical stratosphere isentropic exchange characterized by a PV lamina in 550 to 700 K isentropic levels using the dynamical barrier locating code DYBAL (Dynamical Barrier Localization).

The cause of this transport, where a deformation of PV contours over isentropic surfaces occurs, is explained by planetary wave breaking [55]. The near-stationary mid-latitude winter planetary waves are known to propagate from the troposphere to the stratosphere and meridionally toward the equatorial regions [56]. By E-P flux convergence,

one can identify the breaking of planetary waves, and this can be the cause of several stratospheric isentropic transport events [48,53,57,58].

Air masses originating in the ozone hole passing over middle latitudes were first registered by [59] in the south of Brazil, causing a TCO temporary reduction of about 60 DU for that event. The authors of [60] observed that a 1% TOC reduction in this planet causes a 1.2% ultraviolet radiation (UVR) average increase. Furthermore, the increase in ultraviolet radiation associated with ozone reduction can affect aquatic and terrestrial systems, being one factor that helps to explain the species decline related to malformations caused by an increase in UVR levels [61]. This decline in biodiversity serves to emphasize the importance of these objective studies and the necessity to monitor ozone in these regions.

Furthermore, the observations made by BS for more than twenty years show a good correlation with instruments satellite measurements (~3% differences), with the annual cycle dominating the seasonal variability and interannual variability dominated by quasi-biennial oscillation (QBO), as demonstrated by wavelet analysis and data series comparisons [62]. Climate model projections [63,64] demonstrated that increases in greenhouse gas concentrations result in temperature and stratospheric circulation changes and affect global-scale ozone content.

More recently, using SSO ozone observations [65,66], we identified a significant TOC reduction for October 2016 due to AOH influence that reached Uruguay and Brazil. Similarly, the authors of [67], between 1979 and 2013, also observed 62 events of this type. As an initiative to predict this event's occurrence, the authors of [68] calculated O3 indices that showed great dexterity in representing these events, indicating the polar trough that advanced on southern Brazil with the largest negative O3 anomalies.

This paper analyzes the TOC dataset taken using the BS and OMI instrument satellites, complemented by AURA/MLS ozone profiles followed by MIMOSA model PV fields, to report these polar and middle latitude stratospheric isentropic exchange events from 2005 to 2014. This period covers 10 years of observations from Brewer (since 1992) and AURA/MLS (since the end of 2004), and ozone data from those instruments are simulated by the MIMOSA model to describe the events during this period.

First, the TOC reduction days were selected in the BS and OMI time series. Next, the low-vertical-extension ozone lamina was investigated from the AURA/MLS satellite ozone profiles. Subsequently, an air masses origin diagnosis was conducted by applying the DYBAL code in PV fields by the MIMOSA model to observed reduction levels in AURA/MLS ozone profiles to identify polar origin in these SBAOHI events and determine the dynamic barriers in geographic locations. Finally, the statistics and classification of phenomenon occurrence, summaries, discussion, and conclusions are provided in the last sections.

2. Materials and Methods

2.1. Ozone Experiments

Brewer spectrophotometers (BSs) are fully automated ground-based instruments developed for spectral irradiance measurements in the solar UVB range at five discrete wavelengths, namely, 306.3, 310.1, 313.5, 316.8, and 320.1 nm, with approximately 0.5 nm resolution, allowing nitrogen dioxide (NO_2), sulfur dioxide (SO_2), and ozone (O_3) total column deduction. They can also obtain the atmospheric aerosol optical thickness and ozone profiles by the Umkehr technique [69,70]. The BS TOC observations were conducted from 1992 through the instruments MKIV #081 (1992–1999), MKII #056 (2000–2002), and from 2002 by MKIII #167 in the Southern Space Observatory (SSO) (29.26°S, 53.48°W), Brazil [71], which belongs to the Brazilian Brewer Network.

The Ozone Monitoring Instrument (OMI) is an instrument aboard the AURA satellite, operating since July 2004 in the Earth Observing System (EOS) mission framework. The OMI instrument measures atmospheric components, such as O_3, NO_2, SO_2, and aerosols total column measures, and the data can be downloaded from the NASA website: https://avdc.gsfc.nasa.gov/index.php (accessed on 20 January 2023). OMI performs measurements

through the backscatter ultraviolet technique in two images feeding the spectrometer grid. It has two UV bands, namely, the UV-1 270 at 314 nm and the UV-2 306 at 380 nm, with a 1–0.45 nm spectral resolution [72].

The BS #167 installed in the SSO and OMI instruments during 2005–2014 provides the TOC daily averages analyzed. For this same period, TOC daily averages from OMI instrument satellites were also obtained with the intention of performing a brief comparative analysis, and have a strong correlation between both measurements, as presented in Figure 1, with $R^2 = 0.93$. These results are in line with [62] for the SSO station and other mid-latitude stations around the globe, such as Lauder [49] and the Iberian Peninsula [73], highlighting the confidence of both TOC datasets.

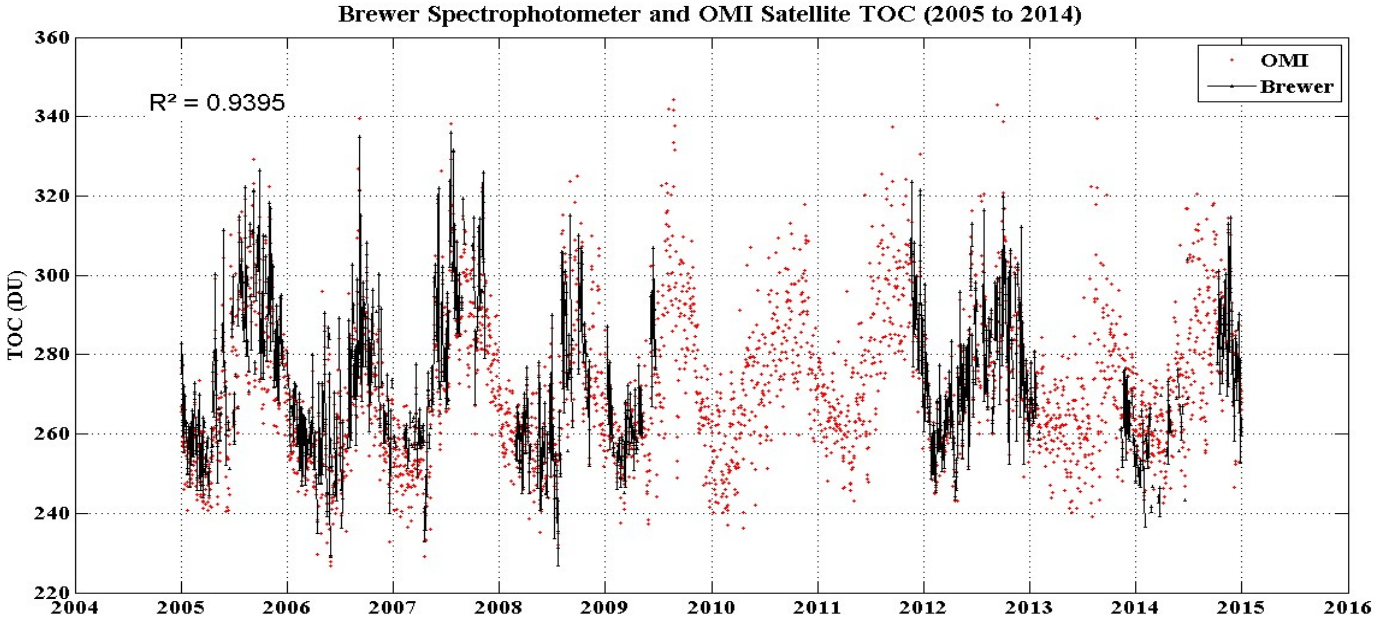

Figure 1. TOC datasets obtained by BS (black) and OMI instrument satellites (red) for the August–November period at the SSO station.

2.2. AURA/MLS Satellite Ozone Profiles Experiment

The AURA/MLS (Microwave Limb Sounder) is an instrument aboard the AURA satellite that participates in the EOS (Earth Observing System) program, was launched in 2004 [74], and maintains a synchronous orbit with the Sun at a near-polar, 700 km altitude and an inclination of 98°. Basic information and v4.3 AURA/MMLS O3 data are available through the following link: http://mls.jpl.nasa.gov/products/o3_product.php (accessed on 20 January 2023). The MLS instrument is capable of providing global coverage between latitudes of ±82° for each day, running around 240 "scans" with each orbit to an extent of about 3500 profiles per day for 17 atmospheric parameters, including ozone, within 41 pressure levels (218–0.01 hPa).

MLS measures microwave thermal emission from the limb and records the vertical profiles of trace gases, including ozone, BrO, ClO, CO, H2O, HCl, HCN, HNO_3, N_2O, and SO_2. Ozone is registered using the 240 GHz spectral region. The MLS vertical resolution ranges are 2.7 km to 3 km from the upper troposphere to the lower mesosphere. For each data acquisition, errors in these measurements must be estimated, and with respect to ozone, error is about ~5–10% range on the stratosphere [75]. Initially, ozone profiles from AURA/MLS version v4.2 were selected in an area ranging from ± 5° latitude and longitude around the SSO region.

From the four ozone profiles closest to the SSO location, daily average profiles were calculated between 2005 and 2014. As these polar vortex disturbances [11,43] related to SBAOHI events are synoptic-scale atmospheric movements, it is possible to analyze this latitude x longitude rang since the interval of 3° × 3° latitude x longitude produces a

daily series with many gaps, which would make it impossible to observe many events. Subsequently, these profiles were interpolated at 350 K to 950 K heights using the same vertical range utilized in PV fields by the MIMOSA model.

2.3. Stratospheric Dynamic Diagnosis by DYBAL Code in MIMOSA Model PV Fields

The MIMOSA (Modélisation Isentrope du transport Mésoéchelle de l'Ozone Stratosphérique par Advection) model is a three-dimensional high-resolution potential vorticity (PV) advection model. This model has been used to study the ozone lamina observed at Observatoire de Haute-Provence (OHP, 44°N, 5.7°E) by LiDAR profiles and to plan the launch of an airborne ozone LiDAR as in [54,76,77]. The dynamical MIMOSA model is particularly used to describe filamentary structure through PV advection, since we can assume that the PV and ozone are very well correlated on an isentropic surface. Consequently, the location of ozone filaments can be determined using PV fields like a dynamical tracer [10,78].

The simulation started at 012 UTC on 1 May 2005, and ended at 012 UTC on 30 November 2014, including the spin-up period (~1 month) on an orthogonal grid in an azimuthal equidistant projection centered at the South Pole (parallels are represented as concentric equidistant circles). The model runs on an isentropic surface and covers the whole Southern Hemisphere, extended between latitudes 10°N and 90°S for a horizontal resolution with an elementary grid cell size of 37 × 37 km (three grid points per degree of latitude).

Meteorological data were obtained at intervals of six hours by the European Center for Medium Range Weather Forecast (ECMWF) analysis at 1.125° latitude × longitude resolution and were provided by the Third European Stratospheric Experiment on Ozone (THESEO) database set up at the Norwegian Institute for Air Research (NILU). Data were first interpolated at a vertical grid spacing that consisted of 25 isentropic vertical levels from 350 K to 950 K with a resolution of 2 km on the fine MIMOSA grid, and, subsequently, PV fields were extracted [40]. The numerical diffusion induced by the regridding processes is minimized by an interpolation scheme that uses the second-order moments of PV [54].

The deformations caused by subtropical and polar vortex barriers are inferred from DYBAL code software using area coordinates and Nakamura's formalism [79]. The DYBAL code aims to localize the dynamic barrier zones in PV fields. The principle is to point out, in a PV field, the regions corresponding to the maximum $\partial PV/\partial A$ (PV gradient) and simultaneously the minimum Le2 (effective diffusivity) for the dynamic barrier locations. Together with a geographic location, DYBAL provides an indication of the strength of these barriers, measured from the secondary maximum PV gradient. This code allows emphasis to be given to the development of polar and subtropical filaments with high precision for their location, as presented in detail by [53].

Having a PV field for time t, first, $\partial PV/\partial \lambda$ and Le2 (λ) are calculated on the basis of equivalent latitude on PV fields; then, the zones of Le2 (λ) minimum and maximum $\partial PV/\partial \lambda$ are digitally detected. A threshold of 1° of equivalent latitude around the maximum and minimum is applied. Throughout this study, PV fields are used at a 1° × 1° resolution and higher than 0.5° of the equivalent latitude threshold. When both criteria are validated (maximum $PV/\partial \lambda$ and Le2 (λ) minimum), the equivalent latitude area is taken as a dynamic barrier that has an error of 1° in estimating the accuracy of the location of the simulated filaments [57].

2.4. Methodology

The first criterion to identify SBAOHI events for 2005–2014 was to look for TOC reduction days measured by BS #167 and the OMI instrument satellite. The criterion adopted should avoid 3% reductions in the monthly climatology, since these types of reductions in TOC can only be caused by tropospheric variations [80]. Considering this, TCO reductions were determined when the TOC daily average value was lower than the -1.5σ limit. These dates with low TOC values were then selected for later verification

of whether air masses came or not from the polar region. The August to November climatological values with their standard deviations and −1.5σ limit for the SSO station, obtained by [62], are shown in Table 1.

Table 1. Climatological values, standard deviations (σ), and −1.5σ limits for the August–November period in the SSO station.

Month	O_3 Climatology in DU (μ)	O_3 SD in DU (σ)	Limit −1.5σ in DU (μ − 1.5σ)
August	284.9	9.1	271.4
September	296.6	9.9	281.7
October	290.2	8.8	277.0
November	286.6	13.0	267.0

We analyzed only the months between August and November because this is the AOH activity period. If the TOC was lower than the −1.5σ limit, this means that if the data were placed over a normal frequency distribution, we would work with the extreme minimum values, representing 6.6% of total days [81]. These TOC reductions cannot be totally credited to tropospheric variations, as photochemistry and transport in the stratosphere are important to explain these reductions, thus supporting the choice of this −1.5σ limit.

The statistical criterion −1.5σ limit was chosen after numerous tests, where it was determined that the mean limit minus one standard deviation (μ-1σ) or mean minus two standard deviations (μ-2σ) could not be used. In the first case, the differences around the average are near to 3%, and these values can be attained by changes in tropospheric ozone. In the last case, only a few days would be analyzed; therefore, proven SBAOHI events would be missed and not analyzed.

From the monthly ozone profile time series, the average, σ, and −1.5σ limits from August to November were calculated. The second criterion was to quantify the stratosphere laminar structure height that causes the TOC reductions observed by the BS and OMI instrument satellites during days with ozone reductions during August to November that were selected in the previous section through the AURA/MLS ozone percent differences profiles between the climatological profile and the reduction day profile, as in Equation (1).

This is the difference between two values divided by their average. Using this gives us the ability to measure the difference between two values (daily and climatology), expressed as a percentage [82]. This technique shows the poor ozone transport levels, demonstrating, with BS, the temporal and vertical ozone content distribution. This information is needed to make the stratospheric dynamic diagnosis that points to these ozone reductions using the MIMOSA model PV field's simulation and the dynamic barrier localization tool, DYBAL code.

The third criterion is to verify the stratospheric 350 to 950 K levels of the MIMOSA model PV fields. This procedure identifies the origin of air masses that cause the TOC reduction measured by the BS and OMI instrument satellites and the ozone profiles measured by the AURA/MLS satellite.

$$Percent\ Difference = 100 * \left(\frac{(Day_i - Climatology_i)}{\left(\frac{(Day_i + Climatology_i)}{2} \right)} \right) \quad (1)$$

These analyses verify if there was some variation in the Absolute PV Fields (APV) MIMOSA model between the reduction days and the previous and posterior days. Therefore, making a vertical and temporal stratospheric dynamic diagnosis is important since an PV increase is a polar origin indication and a decrease indicates that it comes from the equatorial region [48,58]. The DYBAL code is used to check the exact location of subtropical and polar vortex filaments related to the SSO station's geographical position. If the air pollution that causes this ozone depletion is verified, the day is a confirmed SBAOHI event.

Table 2 summarizes ground-based data, satellite data, and model simulation data used in function of the characteristics of each type of data, as well as how to identify SBAOHI events. It should be noted that all datasets used in the analysis were obtained for the period between 2005 and 2014.

Table 2. Type of equipment or model, characteristic of the variable and purpose of using this variable in order to identify SBAOHI events.

Instrument/Model	Characteristics Variable	Propose
BS #167	TCO (DU)	Identify TCO reduction days
OMI	TCO (DU)	Identify TCO reduction days
AURA/MLS	Ozone profiles (ppmv)	Identify the ozone reduction height
DYBAL Code in MIMOSA Model PV Fields	PV fields (PVU)	Identify the air masses origin

3. Results

SBAOHI events between 2005 and 2014 were identified using the three criteria mentioned in the methodology. These criteria are TOC reductions in BS #167 and OMI instrument satellite time series, verification of the MLS ozone profile reduction height, and vertical and temporal stratospheric dynamic analysis by applying DYBAL code in the MIMOSA model PV fields. This is performed to check if air masses are coming from the polar region.

Figure 2 presents the number of August–November observations (blue) and TOC reduction days for August–November (brown) by BS #167 (a) and OMI (b). Large gaps are evident in the Brewer observations between the period from mid-2009 to late 2011, and other shorter gaps are between the end of 2007 and the beginning of 2008 and after 2012. Some of these gaps are due to technical problems such as electronic breakdowns, as described by [62].

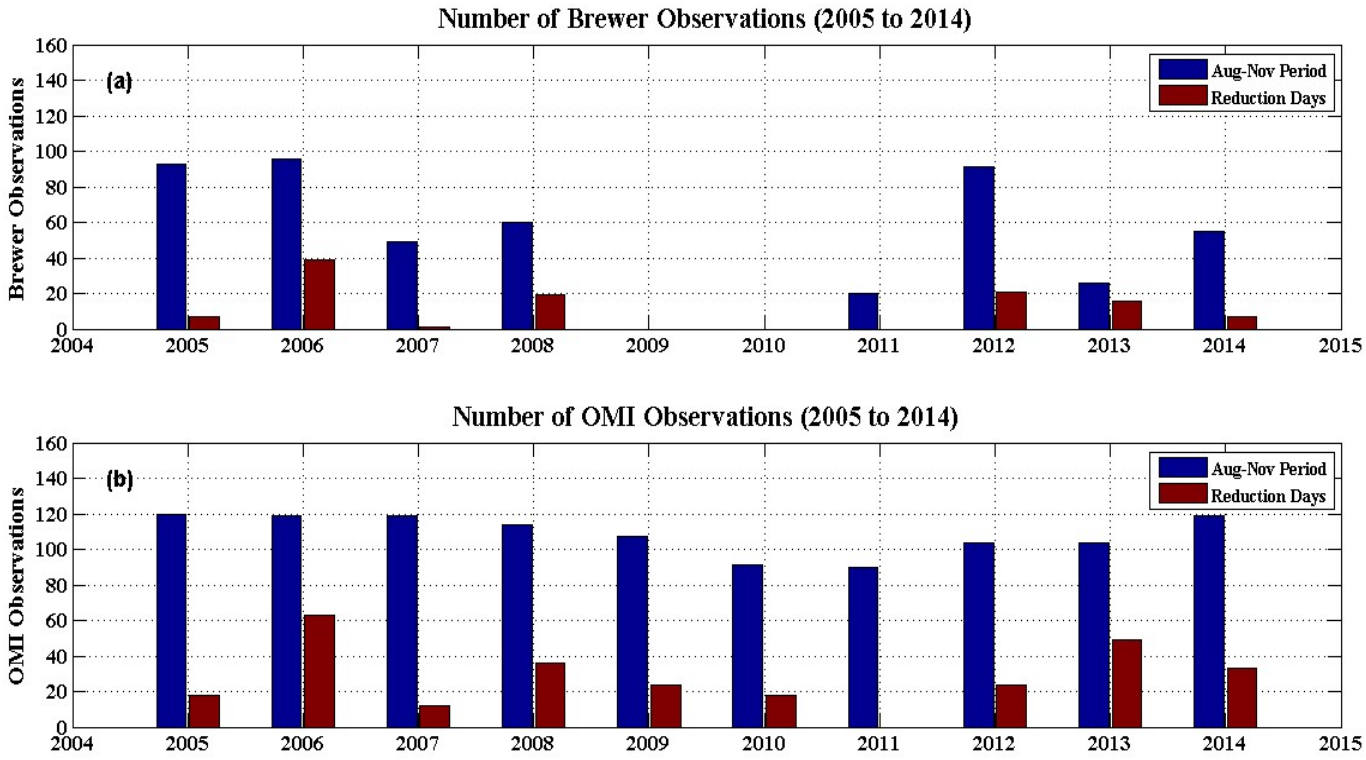

Figure 2. Brewer (**a**) and OMI instrument satellite (**b**) of the August–November observations (blue) and TOC reduction days for August–November (brown) between 2005 and 2014 at the SSO station.

This analysis resulted in 110 days of below-1.5σ limit ozone reduction over the SSO station, with an annual average of 11 days of reduction per year for the August–November period. However, in some cases, due to the closeness of dates, some TOC reduction events may have been counted more than once, and once this had been checked, we confirmed 72 separate events.

Figure 3a shows the BS #167 (in gray) and OMI (in brown) TOC values between August and November 2012, highlighting TOC below the −1.5σ limit (black star line) in blue to identify TOC reduction dates. Figure 3b shows the corresponding time evolution of PV values at the 670 K level (~24 km altitude) on the SSO station. The PV values demonstrate the air polarity over this site. The days with TOC reduction below the −1.5σ limit with a PV values increase, as in around 14 October 2012, were selected to stratospheric vertical MLS ozone profiles with more isentropic trajectories distributions by combining DYBAL contours in the MIMOSA PV fields analyses.

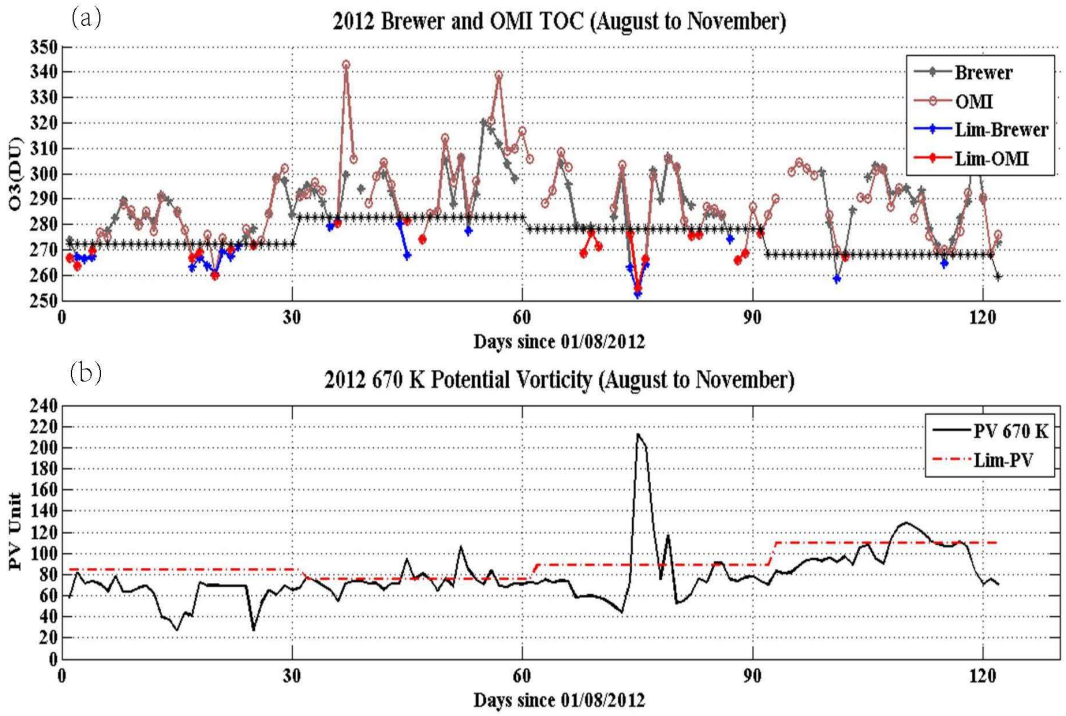

Figure 3. (**a**) TOC of the BS #167 (gray) and OMI instrument satellites (brown) between August and November 2012. Values below the −1.5σ limit (black star line) in blue (Brewer) and red (OMI satellite). (**b**) PV values for the 670 K level (~24 km altitude) between August and November 2012. The dotted black line represents the climatology, and the dotted red line represents the +1.5σ PV values.

In 2012, 33 TOC reduction dates were registered below the −1.5σ limit between August and November. Due to the proximity of the dates, nine (9) possible events were selected, and these days were 6 and 18 August, 5 September, 14 and 22 October, and 10 and 23 November. However, only 23 November did not confirm the SBAOHI event occurrence in both vertical and temporal PV MIMOSA model diagnoses. Polar origin was verified in eight (8) events in 2012, and this was realized for all other years in the 2005–2014 period.

One important event was on 14 October 2012. This case study demonstrates the vertical and temporal stratospheric dynamics diagnosis and confirms the efficiency of this methodology to confirm this event's occurrence.

3.1. Event Study Case

The most significant SBAOHI event observed by BS #167 between 2005 and 2014 was 14 October 2012. This event reached approximately 252.6 DU (Figure 3), representing a

13.4% TOC reduction from October climatology (290.2 ± 8.79 DU), with a PV increase up to 670 K. This case study is an application of the methodology to identify these events.

Figure 4a presents the 14 October 2012 and October climatology ozone profiles obtained by the AURA/MLS satellite instrument as a potential temperature function for the SSO region. Daily TCO reductions are notable when compared to 550 and 700 K levels in October climatology. Figure 4b shows the percent differences in anomalies between the October climatology ozone profile and daily ozone profiles between 10 and 16 October 2012. Anomaly profiles with a reduction from 10 October are observed. This reached values lower than −20% on 14 October at 550 and 700 K laminas, and this reduction can still be observed, although it became less intense on subsequent days.

The DYBAL code applied to the MIMOSA model PV fields is used to verify where the maximum PV gradient (∂PV/∂A) and minimum simultaneous effective diffusivity (Le2) are found. This procedure detects subtropical and polar dynamic barrier positions [79,83]. The subtropical (red line) and polar (black line) barrier positioning, calculated by the DYBAL code, and the SSO region (black X) are presented through vertical (Figure 5) and temporal (Figure 6) stratospheric dynamics diagnosis in the MIMOSA PV fields.

This analysis is performed to identify the origin of the air masses arriving at the SSO station on the selected reduction days where ozone depletion laminas in the AURA/MLS satellite profiles were found. The vertical DYBAL output distribution in the MIMOSA PV fields for 400, 450, 500, 525, 675, and 850 K levels for the 14 October 2012 event is presented in Figure 5.

That objective is to verify the stratospheric vertical structure during the occurrence of events. To classify whether these are polar filaments or polar tongues in the MIMOSA PV fields, it was assumed that a polar filament occurs when only PV filaments are observed, but a polar tongue occurs when a large PV filament surrounded by a polar barrier line in the SSO region is observed.

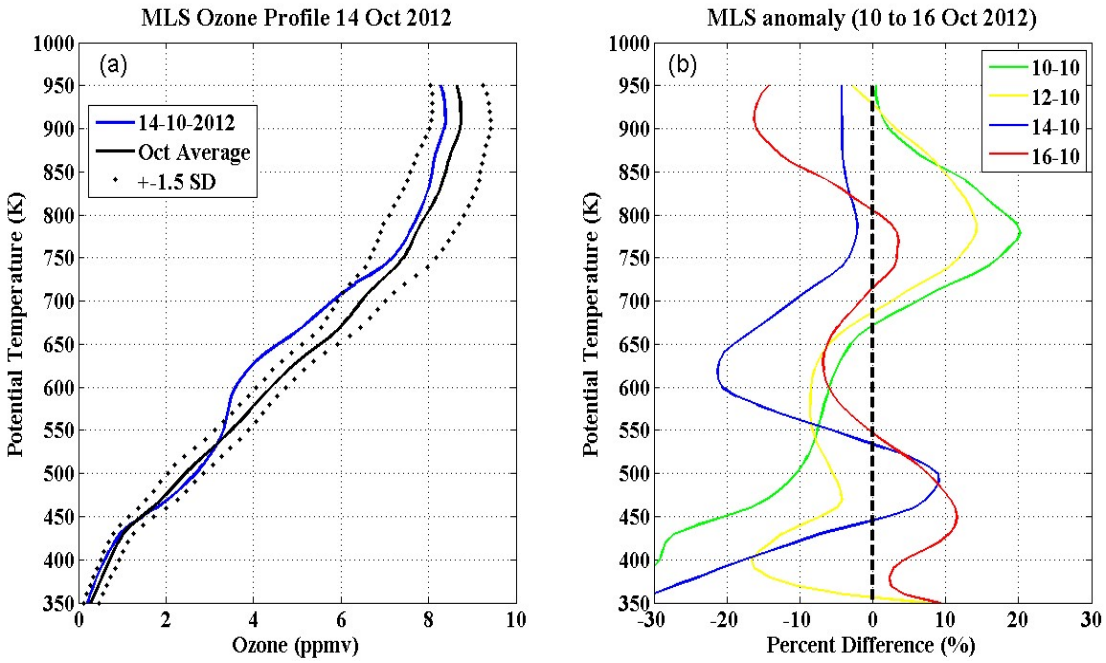

Figure 4. (**a**) Comparison of the AURA/MLS satellite ozone profiles for 14 October 2012 in blue and the October climatology ozone profile (black). Dotted lines correspond to the ±1.5σ October climatology limit. (**b**) Percent ozone anomalies, derived as differences between monthly and daily ozone recorded on 10, 12, 14, and 16 October 2012. The dotted black line represents the null difference.

In the SSO region, the 400 K level shows the subtropical barrier. From 450 to 525 K levels, polar origin is observed due to the higher PV values presence as a polar filament.

From 675 to 850 K levels, a very intense polar tongue with a higher PV value has a polar barrier. These results give indications of intense transport from the polar region toward the subtropics.

Figure 5 shows that above the 500 K level, the high PV values of polar tongue positioning in the study area are more evident at 675 K. This corroborates the largest AURA/MLS ozone profile negative anomaly observed, as shown in Figure 4. Additionally, a temporal analysis at this isentropic level (675 K) using the DYBAL outputs (dynamical barrier locations) superimposed with the corresponding MIMOSA model PV fields before and after the "14 October event" was performed.

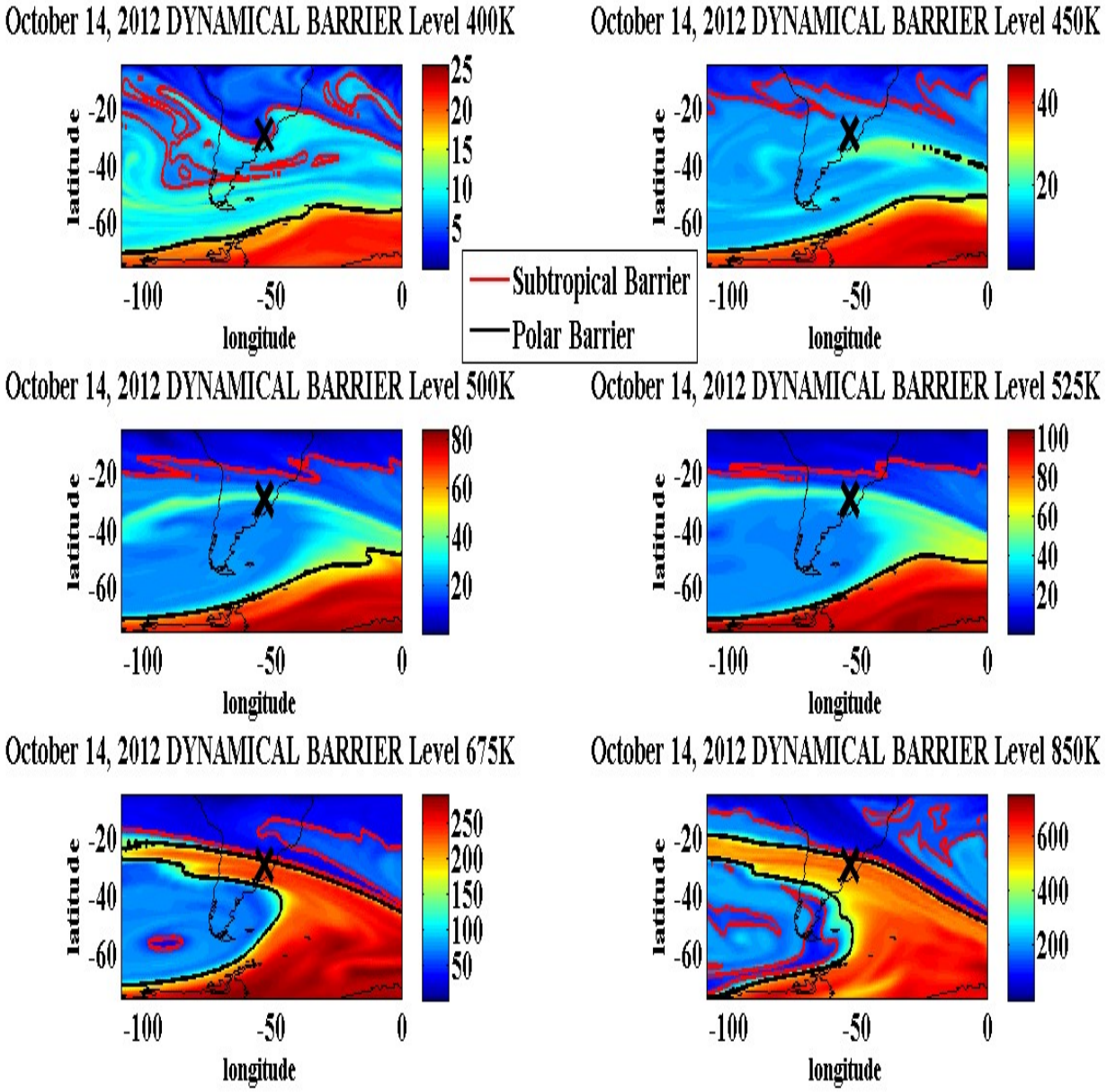

Figure 5. Vertical evolution of the MIMOSA model PV fields on stratospheric isentropic surfaces (400, 450, 500, 525, 675, and 850 K) on 14 October 2012. Locations of dynamical barriers (subtropical barrier in red and polar barrier in black) are overlapped on the maps using a color scale with PV units. The X indicates the SSO location.

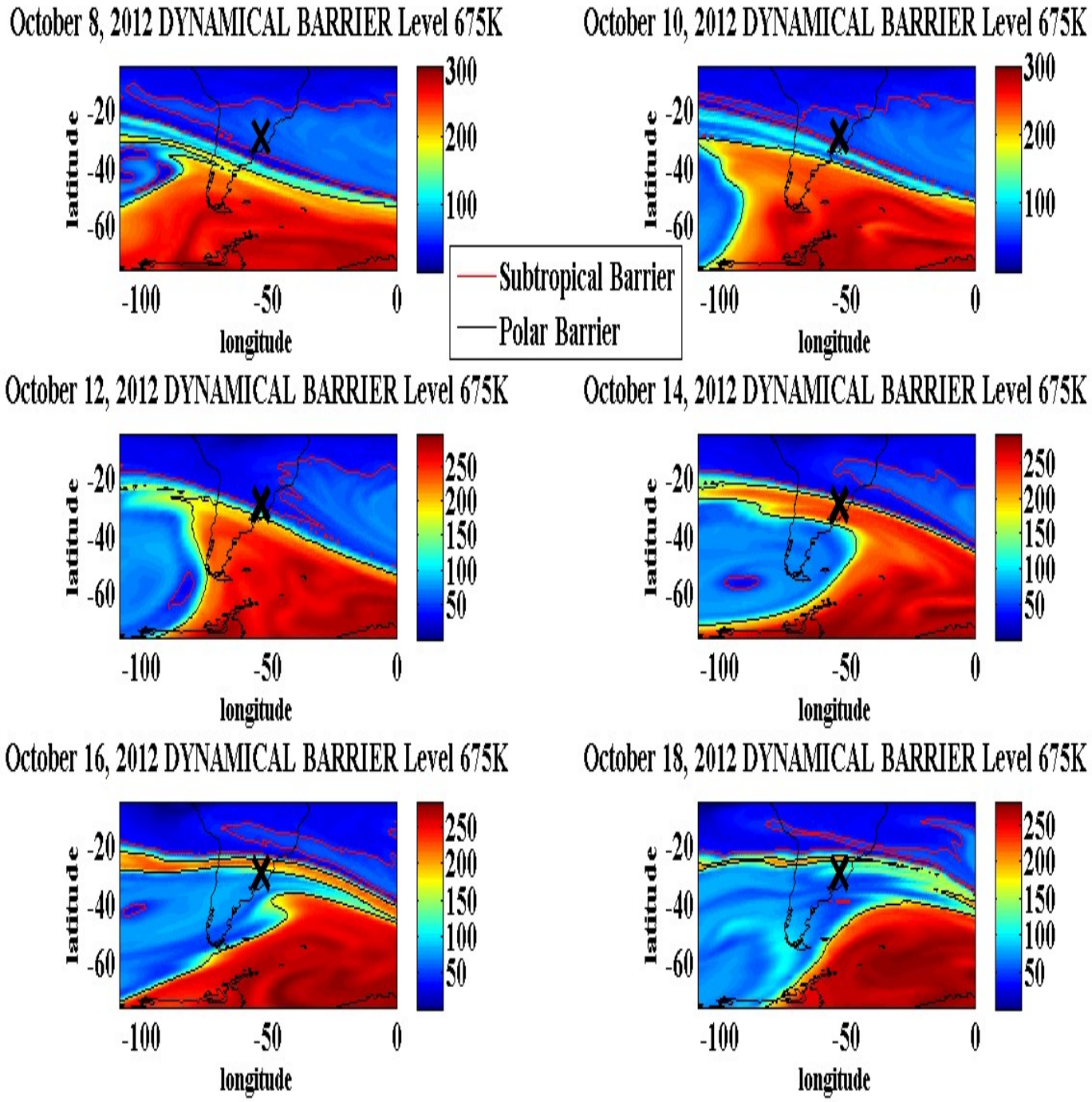

Figure 6. Temporal evolution of MIMOSA model PV fields for a 675 K isentropic surface obtained on 8, 10, 12, 14, 16, and 18 October. Locations of dynamical barriers (subtropical barrier in red and polar barrier in black) are overlapped on the maps using a color scale with PV units. The X indicates the SSO location.

Figure 6 shows an intensely higher PV polar tongue presence surrounded by a polar barrier line over Central and Southern Argentina on 8 October. This polar tongue moves northward and reaches the SSO station on 14 October, moving further north and losing intensity on 16 October in the Atlantic Ocean, causing the observed reductions in BS #167 and OMI TOC and in the AURA/MLS satellite ozone profile during this period.

These results are explained by studies on polar filamentation effects in the mid-latitude stratosphere caused by transport between pole and mid-latitude mixing zones conducted

by [54,84]. In addition, our results are consistent with previously reported disturbances caused by AOH influence events on 30°S [59] and polar filaments over mid-latitude sites reported by [41]. This analysis shows that the intense polar tongue of high PV values surrounded by the polar barrier was ejected in the direction of southern Brazil, confirming the event that occurred on 14 October 2012.

3.2. Statistics and Classification of SBAOHI Events between 2005 and 2014

When applying the same methodology used in 2012 for the 2005–2014 period, the TOC reduction days resulted in 110 days below the -1.5σ limit, with an annual average of 11 days of TOC reduction per year. However, in terms of proximity dates, TOC reductions can be caused by the same polar transport. A total of 72 possible events were separated, of which 62 were confirmed by the vertical and temporal stratospheric dynamics diagnosis.

This analysis is performed by detecting the AURA/MLS satellite ozone profiles, lamina reduction height, transport from the AOH to the SSO station, and dynamic barriers position verification from the DYBAL code applied in the MIMOSA model PV fields. Fewer than 15% (13.8%) of ozone reduction events were not confirmed as being due to SBAOHI events. A summary of the 62 confirmed SBAOHI events between 2005 and 2014 is presented in Table S1 in the Supplementary Material. This synthesizes the event occurrence dates, the TOC values, the percent reduction respective to monthly climatology, the isentropic level of the AURA/MLS satellite ozone profile reduction, and their maximum percent reduction.

Additionally, the characteristics and levels of polar transport to the SSO station region through the application of the DYBAL code in the MIMOSA model PV fields are presented. Thus, polar filaments (PV filament only) or polar tongues (PV filament plus Polar Barrier DYBAL line) in PV fields are detected in all events that occurred in the 2005–2014 period.

SBAOHI events occur on average 6.2 ± 2.6 times per year, with mean TOC reductions registered by BS #167 of $7.0 \pm 2.9\%$ and $7.7 \pm 2.4\%$ for the OMI satellite. Furthermore, the mean isentropic level (K) and maximum mean AURA/MLS ozone profile reduction occurred at 640 ± 150 K and $15.3 \pm 6.3\%$, respectively. In October, there are 19 events in total (30.7%), followed by September with 18 (29.1%), August with 14 (22.5%), and November with 11 (17.7%). Overall, only 19.3% of events showed polar tongue structures, while 80.7% of events presented polar filament structures.

In 400 K, only 4.89% of total events occur, while 10.48% occur at 450 K, 14.68% at 500 K, 18.88% at 600 K, 27.97% at 675 K, and 23.07% at 850 K. This kind of isentropic analysis allows the seasonal and geographical variability of the filament preferred forms of exchange identification [85] through nitrous oxide (N_2O) laminar structures from a stratospheric three-dimensional chemical transport model, where during the winter and boreal spring, these structures are introduced from middle latitudes to the tropics. Using our analysis, we emphasize 500 to 850 K as the preferential levels of stratospheric transport with observed ozone depletion lamina when there are SBAOHI events.

This event's occurrences are separate per year and month and illustrated in Figure 7. With 10 events, 2006 stands out as the year of greatest event occurrence, being 3 in August, 2 in September, 3 in October, and 2 in November. This is explained because 2006 recorded the largest AOH area in history (https://www.theozonehole.org/ozoneholehistory.htm) (accessed on 20 January 2023).

Events were classified into three categories by taking into account (1) TOC reduction from BS #167 and OMI records intensity, (2) reduction lamina height determined from the corresponding AURA/MLS ozone profile, and (3) the event dynamical shape form of a filament or tongue structure identified from DYBAL code and MIMOSA PV maps.

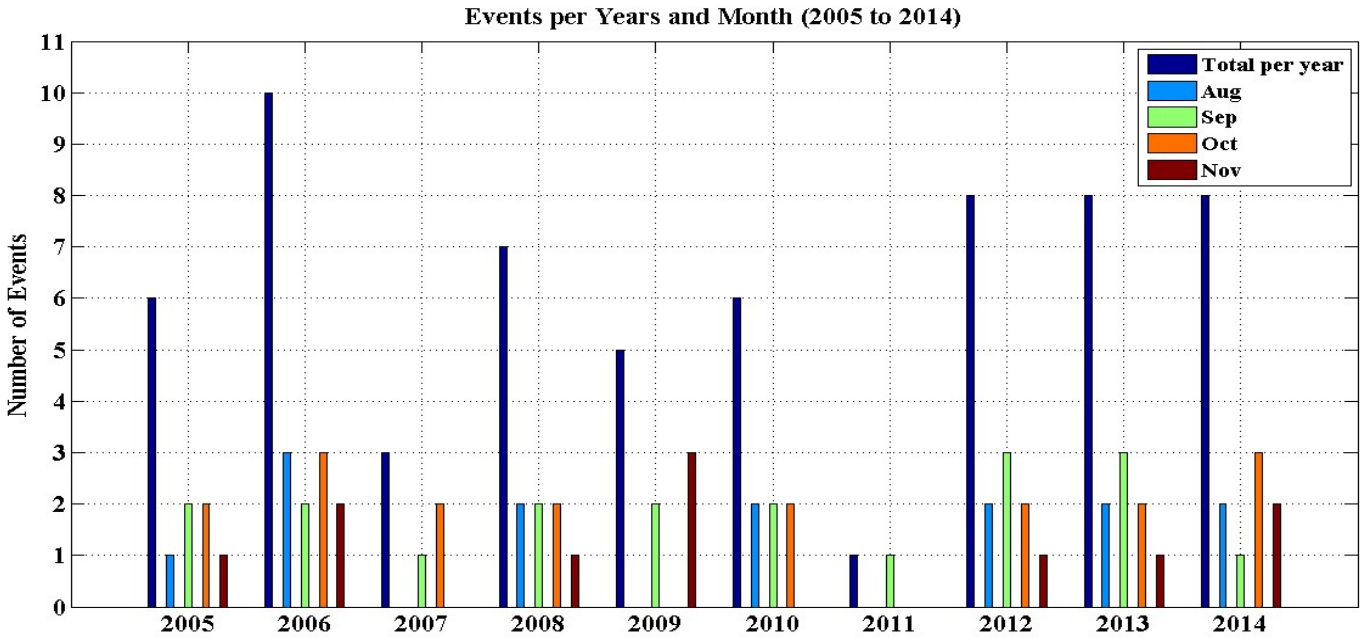

Figure 7. Time distribution of the number of SBAOHI events per month and per year between 2005 and 2014.

Three intensity levels have been defined according to the TOC reduction percentage (%): minor when %TOC is less than 6% (%TOC < 6%), medium when %TOC is between 6 and 9% (6% $\leq$ %TOC < 9%), and major when %TOC is greater than or equal to 9% (%TOC $\geq$ 9%).

The isentropic heights of occurrence events were divided into three layers: low stratosphere (LS) for X < 500 K; medium stratosphere (MS) for 500 K $\leq$ X < 700 K; and upper stratosphere (US) when X $\geq$ 700 K. It should be noted that an event can be identified by more than one height category.

Figure 8 shows plots of monthly ozone reduction event percentages and occurrences. The upper plots, Figure 8a,b, illustrate event statistics with a "tongue" structure, while the lower plots, Figure 8c,d, show distributions of events characterized by a "filament" structure. Moreover, the plots on the left side of Figure 8 show the event distribution according to their intensity (minor, medium, or major); the plots on the right side indicate how the events are distributed in the three stratospheric layers (LS, MS, and US).

Polar tongue characteristics were observed only in 19.3% (12 events): 1 in August (8.4% of cases), 2 in September (16.6% of cases), 6 in October (50% of cases), and 3 in November (25% of cases), with medium intensity (58.2% of cases) and stratosphere medium levels (55.0% of cases). Polar filament characteristics were observed in 80.7% of total cases and are distributed in 26.0% of cases in August, 32.0% in September, 26.0% in October, and 16.0% in November, with medium intensity (42.0% of cases) and in the stratosphere (40.7% of cases).

These results are consistent with [54,86], who used the MIMOSA model to identify the polar air presence in the medium-latitude lower stratosphere (about 450 K). The simulation results allowed for interpretation of the laminar structures observed in vertical ozone profiles measured by the LiDAR in the Observatory of Haute Provence (OHP).

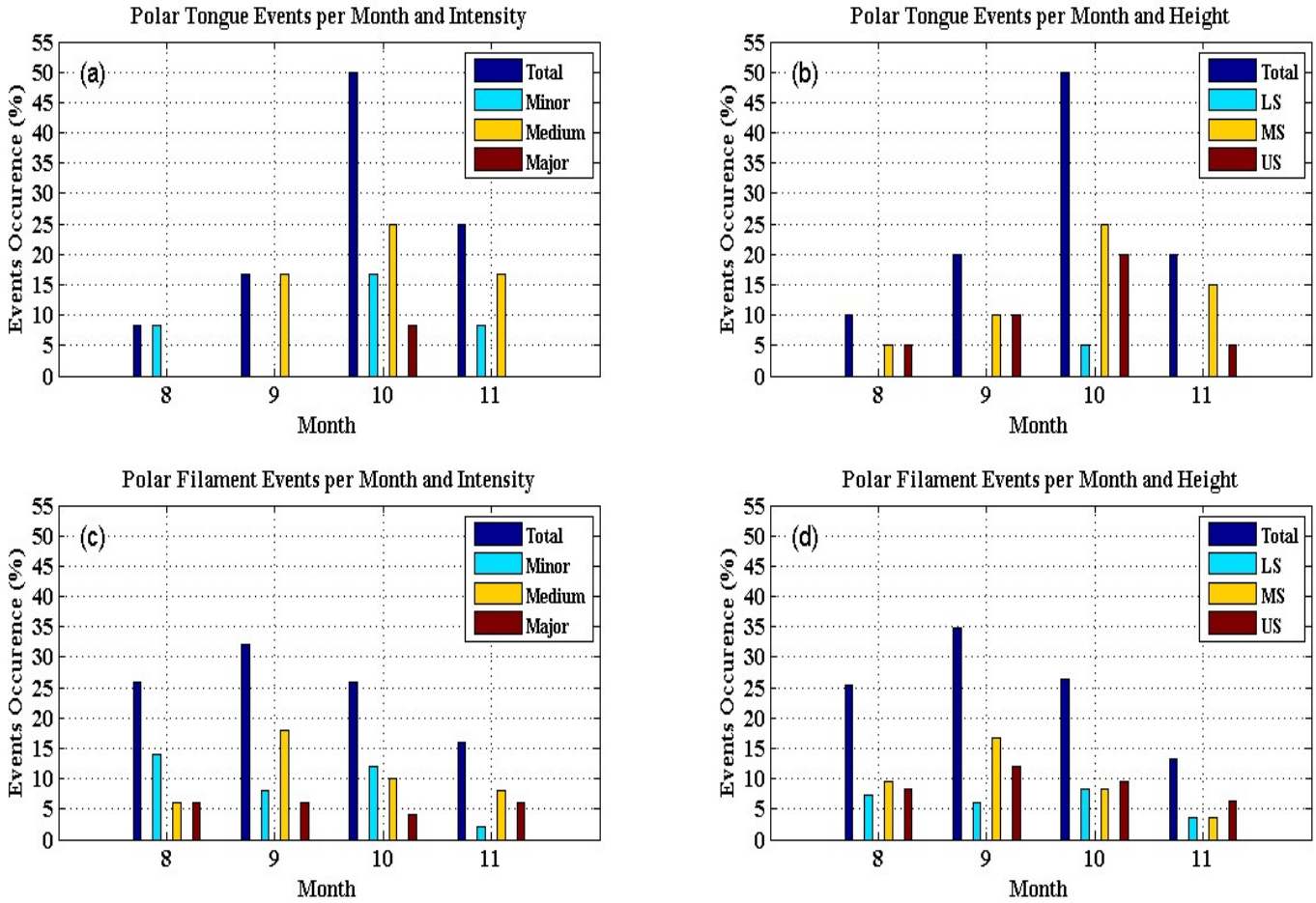

Figure 8. Frequency of occurrence (percentage) of SBAOHI events per month. The upper plots, (**a**,**b**), illustrate the events with "tongue" structure statistics, while the lower plots, (**c**,**d**), present the "filament" structure events between 2005 and 2014.

4. Discussion

The observation, remote sensing, and numerical simulation used to identify and characterize SBAOHI events between 2005 and 2014 demonstrate their importance since this type of phenomenon causes ~10% temporary TOC reductions [67]. This can reach dangerous RUV levels since this increase is 1.2% for every 1% TOC reduction over southern Brazil [60]. Furthermore, this is associated with one of the causes that explain the reduction of two species of small frogs in this region [61].

The authors of [62] presented a detailed description of TOC monitoring using BS, TOMS, and OMI satellite instruments in SSO for more than 20 years (1992–2014) and gave a comparison with satellite measurements (<3% differences). These determine the seasonal variability that dominates the annual cycle, with a minimum (~260 DU) in April and a maximum (~295 DU) in September. Interannual variability is dominated by quasi-biennial oscillation (QBO) mode, identified by wavelet analysis and comparing the QBO index with the monthly TOC anomaly time series, and a condition of a near antiphase was described by these instruments. TOC from OMI has a good correlation with other TOC measurements observations in the southern subtropics by Dobson and SAOZ spectrometers and ozone profiles [87,88], in addition to IASI European satellite instruments [89].

After this knowledge about observational and remote sensing TOC time series comparisons and variability analysis, identifying and characterizing better SBAOHI events has been gaining importance, as in the major event observed in October 2016, where the reduction in TCO was ~23% [66]. This event was also observed by multi-instrumental

data, including the ozone-sounding balloon that observed a ~60% reduction at 24.5 km height [65].

Additionally, the authors of [53] demonstrated that deformation on a planetary scale led to the intrusion of tropical air tongues towards mid-latitudes and numerically simulated the large-scale isentropic transport that increased the ozone over Reunion Island (55°E, 21°S). This result was due to the mid-latitudes in the tropical stratosphere air masses displacement onto the ozone lamina, and the DYBAL code was used to identify the dynamic barriers positioning in the MIMOSA model.

This has been encouraging new studies that aim to simulate and predict these events [68], using deep learning [90] and a new dataset, ERA-5 reanalysis [91], to investigate the long-term atmospheric dynamics behavior [92]. In October 2015, these events led to a +16.6 ± 54.6% UVI increase, even with a predominance of partly cloudy days [93]. All these factors corroborate the importance of the analysis carried out in this work.

5. Conclusions

This paper presents the SBAOHI event occurrence between 2005 and 2014 observed by the BS #167, OMI, and AURA/MMLS satellites and simulated by applying the DYBAL code in the MIMOSA model PV fields. This was performed to verify the temporal and vertical distribution and intensity of TOC reductions. Atmospheric dynamic characteristics and climatic indexes such as QBO and ENSO influence during this phenomenon occurrence were identified.

The BS #167 and OMI satellite TOC on the SSO station were compared in the 2005–2014 period, and a good correlation (R^2 = 0.93) was obtained between the instruments. Thus, validated TOC from both instruments was used for the first stage to identify the SBAOHI event occurrence. In total, 110 ozone reduction days were selected in the August–November period, with an average of 11 days per year. However, due to the proximity of the dates, 72 possible events were selected for air mass origin analysis. It must be noted that the number of days with data is different depending on the considered year.

The 14 October 2012 event was taken as an example of applying this methodology to identify the events. This is the most significant BS event in the period 2005–2014 since it presented a 252.6 DU TOC value, a 13.4% reduction compared to the October average (290.2 ± 8.79 DU). The AURA/MMLS satellite ozone profile obtained on 14 October 2012 for the SSO region showed a substantial ozone reduction (~20%) in relation to the October ozone profile for 550 at 700 K levels.

In addition, vertical and temporal stratosphere dynamics diagnosis provided by the application of the DYBAL code in the MIMOSA model PV fields showed an intense polar tongue of high PV values in the isentropic surfaces of 670 and 850 K passing on the SSO station region.

Applying the same methodology, 62 SBAOHI events were confirmed. This event occurred 6.2 ± 2.6 times per year average, with mean TOC reductions by BS #167 of 7.0 ± 2.9% and OMI satellite of 7.7 ± 2.4%. In the AURA/MLS satellite, the mean isentropic level and maximum mean ozone profile reduction occurred at 640 ± 150 K and 15.3 ± 6.3%, respectively, ensuring that this kind of phenomenon is important when ozone reduction occurs in the SSO region. Between 500 and 850 K levels, these events were identified using the DYBAL code in the MIMOSA model PV fields.

October is the month with the most events, with 19 in total (30.7%), followed by September with 18 (29.1%), and 19.3% showed the polar tongue atmospheric characteristic, while 80.7% presented the polar filament atmospheric characteristic. The 500 and 850 K levels were shown as the preferential levels of stratospheric transport during SBAOHI events. The year 2006 was the year with the most events in a single year (10), while 2011 showed fewer events in a single year (1), and from 2012 to 2014, eight events occurred per year.

The events were separated into three categories: TOC reduction intensity, height of reduction lamina in the ozone profile, and filaments or tongues as atmospheric dynamic

characteristics. Only 19.3% of total cases were polar tongue, and these were more frequent in October (50%), with medium intensity (58.2%), and in the stratosphere (55.0%) in the majority of cases. Polar filament events (80.7%) were more frequent in September (32.0%), with medium intensity (42.0%), and in the stratosphere, with medium level (40.7%) in the majority of cases.

Supplementary Materials: The following supporting information can be downloaded at: https://www.mdpi.com/article/10.3390/rs16112017/s1. Table S1. Dates of events of influence of the Antarctic ozone hole on the SSO station and respective value of Brewer's TOC, its reduction percentage in relation to monthly climatology, and the isentropic level of ozone reduction in the profile of the AURA satellite/MLS. The layer of the largest reduction and the percentage of this reduction, in addition to the level and characteristic of the polar transport observed towards the region of the SSO station. (-) Indicates that there was no observation by the instrument.

Author Contributions: Conceptualization, L.V.P., D.K.P., H.B., T.P., J.V.B., V.A. and N.B.; methodology, L.V.P., D.K.P., H.B., N.M., T.P., G.D.B., T.T.d.A.T.N., M.A.T., A.P.S. and R.P.T.S.; software and hardware, L.V.P., L.A.S., R.P.T.S., M.A.G.d.R., G.D.B., M.A.T. and N.M.; formal analysis, L.V.P.; data curation, L.V.P., G.D.B., D.K.P., J.V.B. and M.P.P.M.; writing—original draft preparation, L.V.P.; writing—review and editing, L.V.P., G.C.G.d.R., G.D.B., J.V.B., R.d.S., D.K.P., H.B., N.M., M.A.T., M.P.P.M., L.A.S., N.B., T.T.d.A.T.N., V.A., A.P.S. and D.M.; funding acquisition, L.V.P., D.K.P., H.B., R.d.S., M.P.P.M. and D.M. All authors have read and agreed to the published version of the manuscript.

Funding: CAPES (Coordination for the Improvement of Higher Education Personnel), a foundation linked to the Brazilian Ministry of Education, and COFECUB (French Evaluation Committee of the University and Scientific Cooperation with Brazil), project number 88887.130199/2017-01.

Data Availability Statement: Data available on request from L.P.

Acknowledgments: The MESO Project from CAPES/COFECUB Program (Process No. 88887.130176/2017-01), at Federal University of Western Pará (UFOPA), Federal University of Santa Maria (UFSM), with the Laboratory of Atmosphere and Cyclones (LACy) on University of Reunion Island (France). The authors also thank the NASA/TOMS/OMI for the data used in the analysis.

Conflicts of Interest: The authors declare no conflicts of interest.

References

1. Gettelman, A.; Hoor, P.; Pan, L.L.; Randel, W.J.; Hegglin, M.I.; Birner, T. The Extratropical Upper Troposphere and Lower Stratosphere. *Rev. Geophys.* **2011**, *49*, RG3003. [CrossRef]
2. Bracci, A.; Cristofanelli, P.; Sprenger, M.; Bonafè, U.; Calzolari, F.; Duchi, R.; Laj, P.; Marinoni, A.; Roccato, F.; Vuillermoz, E.; et al. Transport of Stratospheric Air Masses to the Nepal Climate Observatory-Pyramid (Himalaya; 5079 m MSL): A Synoptic-Scale Investigation. *J. Appl. Meteorol. Clim.* **2012**, *51*, 1489–1507. [CrossRef]
3. Brewer, A.W. Evidence for a world circulation provided by the measurements of helium and water vapour distribution in the stratosphere. *Q. J. R. Meteorol. Soc.* **1949**, *75*, 351–363. [CrossRef]
4. Dobson, G.M.B. Forty years' research on atmospheric ozone at Oxford: A history. *Appl. Opt.* **1968**, *7*, 387–405. [CrossRef]
5. Roscoe, H.K. The Brewer–Dobson circulation in the stratosphere and mesosphere—Is there a trend? *Adv. Space Res.* **2006**, *38*, 2446–2451. [CrossRef]
6. Weber, M.; Dikty, S.; Burrows, J.P.; Garny, H.; Dameris, M.; Kubin, A.; Abalichin, J.; Langematz, U. The Brewer-Dobson circulation and total ozone from seasonal to decadal time scales. *Atmos. Chem. Phys.* **2011**, *11*, 11221–11235. [CrossRef]
7. Schoeberl, M.R. Reconstruction of the constituent distribution and trends in the Antarctic polar vortex from ER-2 flight observations. *J. Geophys. Res. Atmos.* **1989**, *94*, 16815–16845. [CrossRef]
8. Danielsen, E.F. Stratospheric-tropospheric exchange based upon radioactivity, ozone and potential vorticity. *J. Atmos. Sci.* **1968**, *25*, 502–518. [CrossRef]
9. Larry, D.; Chipperfild, M.; Pyle, J.; Norton, W.; Riishojgaard, L. Tree-dimensional tracer initialization and general diagnostics using equivalent PV latitude-potential-temperature coordinates. *Q. J. R. Meteorol. Soc.* **1995**, *121*, 187–210. [CrossRef]
10. Hoskins, B.J.; McIntyre, M.E.; Robertson, A.W. On the use and significance of isentropic potential vorticity maps. *Q. J. R. Meteorol. Soc.* **1985**, *111*, 877–946. [CrossRef]
11. Norton, W.A. Breaking Rossby waves in a model stratosphere diagnosed by a vortex–following coordinate system and a technique for advecting material contours. *J. Atmos. Sci.* **1994**, *51*, 654–673. [CrossRef]

12. Nash, E.R.; Newman, P.A.; Rosenfield, J.E.; Schoeberl, M.E. An objective determination of the polar vortex using Ertel's potential vorticity. *J. Geophys. Res. Atmos.* **1996**, *101*, 9471–9478. [CrossRef]
13. Marchand, M.; Bekki, S.; Pazmiño, A.; Lefèvre, F.; Godin, S.; Hauchecorne, A. Model simulations of the impact of the 2002 Antarctic ozone hole on midlatitudes. *J. Atmos. Sci.* **2005**, *62*, 871–884. [CrossRef]
14. Trepte, C.R.; Hitchman, M.H. Tropical stratospheric circulation deduced from satellite aerosol data. *Nature* **1992**, *355*, 626–628. [CrossRef]
15. Grant, W.B.; Browell, E.V.; Long, C.S.; Stowe, L.L.; Grainger, R.G.; Lambert, A. Use of volcanic aerosols to study the tropical stratospheric reservoir. *J. Geophys. Res. Atmos.* **1996**, *101*, 3973–3988. [CrossRef]
16. Chubachi, S. Preliminary result of ozone observations at Syowa Station from February, 1982 to January, 1983. *Mem. Natl. Inst. Polar Res. Jpn. Spec.* **1984**, *34*, 13–20. Available online: http://id.nii.ac.jp/1291/00001666/ (accessed on 15 February 2023).
17. Farman, J.C.; Gardiner, B.G.; Shanklin, J.D. Large losses of total ozone in Antarctica reveal seasonal ClOx/NOx interaction. *Nature* **1985**, *315*, 207–210. [CrossRef]
18. Solomon, S. Stratospheric ozone depletion: A review of concepts and history. *Rev. Geophys.* **1999**, *37*, 275–316. [CrossRef]
19. Schoeberl, M.R.; Hartman, D.L. The dynamics of the stratospheric polar vortex and its relation to springtime ozone depletions. *Science* **1991**, *251*, 46–52. [CrossRef]
20. Roscoe, H.K.; Feng, W.; Chipperfield, M.P.; Trainic, M.; Shuckburgh, E.F. The existence of the edge region of the Antarctic stratospheric vortex. *J. Geophys. Res. Atmos.* **2012**, *117*, D04301. [CrossRef]
21. Solomon, S.; Garcia, R.R.; Rowland FS Wuebbles, D.J. On the depletion of Antarctic ozone. *Nature* **1986**, *321*, 755–758. [CrossRef]
22. Lambert, A.; Santee, M.L.; Wu, D.L.; Chae, J.H. A-train CALIOP and MLS observations of early winter Antarctic polar stratospheric clouds and nitric acid in 2008. *Atmos. Chem. Phys.* **2012**, *2*, 2899–2931. [CrossRef]
23. Hofmann, D.J.; Oltmans, S.J.; Harris, J.M.; Johnson, B.J.; Lathrop, J.A. Ten years of ozone sonde measurements at the South Pole: Implications for recovery of springtime Antarctic ozone. *J. Geophys. Res. Atmos.* **1997**, *102*, 8931–8943. [CrossRef]
24. Müller, R.; Grooß, J.U.; Lemmen, C.; Heinze, D.; Dameris, M.; Bodeker, G. Simple measures of ozone depletion in the polar stratosphere. *Atmos. Chem. Phys.* **2008**, *8*, 251–264. [CrossRef]
25. Salby, M.L.; Titova, E.A.; Deschamps, L. Changes of the Antarctic ozone hole: Controlling mechanisms, seasonal predictability, and evolution. *J. Geophys. Res. Atmos.* **2012**, *117*, D10111. [CrossRef]
26. Lefèvre, F.; Figarol, F.; Carslaw, K.S.; Peter, T. The 1997 Arctic Ozone depletion quantified from three-dimensional model simulations. *Geophys. Res. Lett.* **1998**, *25*, 2425–2428. [CrossRef]
27. Tripathi, O.P.; Godin-Beekmann, S.; Lefèvre, F.; Marchand, M.; Pazmiño, A.; Hauchecorne, A.; Goutail, F.; Schlager, H.; Volk, C.M.; Johnson, B.; et al. High resolution simulation of recent Arctic and Antarctic stratospheric chemical ozone loss compared to observations. *J. Atmos. Chem.* **2006**, *55*, 205–226. [CrossRef]
28. Solomon, S.; Portmann, R.W.; Thompson, D.W.J. Contrasts between Antarctic and Arctic ozone depletion. *Proc. Natl. Acad. Sci. USA* **2007**, *104*, 445–449. [CrossRef]
29. Newman, P.A.; Nash, E.R. Quantifying the wave driving of the stratosphere. *J. Geophys. Res. Atmos.* **2000**, *105*, 12485–12497. [CrossRef]
30. Zerefos, C.S.; Tourpali, K.; Bojkov, B.R.; Balis DS Rognerund, B.; Isaksen, I.S.A. Solar activity-total ozone relationships: Observations and model studies with the heterogeneous chemistry. *J. Geophys. Res. Atmos.* **1997**, *102*, 1561–1569. [CrossRef]
31. Chipperfield, M.P.; Jones, R.L. Relative influences of atmospheric chemistry and transport on Arctic ozone trends. *Nature* **1999**, *400*, 551–555. [CrossRef]
32. Kuttippurath, J.; Lefèvre, F.; Pommereau, J.-P.; Roscoe, H.K.; Goutail, F.; Pazmiño, A.; Shanklin, J.D. Antarctic ozone loss in 1979–2010: First sign of ozone recovery. *Atmos. Chem. Phys.* **2013**, *13*, 1625–1635. [CrossRef]
33. Solomon, S.; Ivy, D.J.; Kinnison, D.; Mills, M.J.; Neely, R.R.; Schmidt, A. Emergence of healing in the Antarctic ozone layer. *Science* **2016**, *353*, 269–274. [CrossRef]
34. Kirchhoff, V.W.J.H.; Sahai, Y.; Casiccia CA, R.; Zamorano, F.; Valderrama, V. Observations of the 1995 ozone hole over Punta Arenas, Chile. *J. Geophys. Res. Atmos.* **1997**, *102*, 16109–16120. [CrossRef]
35. Perez, A.; Jaque, F. On the Antarctic origin of low ozone events at the South American continent during the springs of 1993 and 1994. *Atmos. Environ.* **1998**, *32*, 3665–3668. [CrossRef]
36. Pazmino, A.F.; Godin-Beckmann, S.; Ginzburg, M.; Bekki, S.; Hauchecorne, A.; Piacentini, R.D.; Quel, E.J. Impact of Antarctic polar vortex occurrences on total ozone and UVB radiation at southern Argentinean and Antarctic stations during 1997–2003 period. *J. Geophys. Res. Atmos.* **2005**, *110*, D03103. [CrossRef]
37. de Laat, A.T.J.; van der A, R.J.; Allaart, M.A.F.; van Weele, M.; Benitez, G.C.; Casiccia, C.; Leme, N.M.P.; Quel, E.; Salvador, J.; Wolfram, E. Extreme sunbathing: Three weeks of small total O-3 columns and high UV radiation over the southern tip of South America during the 2009 Antarctic O-3 hole season. *Geophys. Res. Lett.* **2010**, *37*, L14805. [CrossRef]
38. Schoeberl, M.R.; Lait, L.R.; Newman, P.A.; Rasenfield, J.E. The structure of the polar vortex. *J. Geophys. Res. Atmos.* **1992**, *97*, 7859–7882. [CrossRef]
39. Waugh, D.; Plumb, R.; Atkinson, R.J.; Schoeberl, M.R.; Lait, L.R.; Newman, P.A.; Loewenstein, M.; Toohet, D.; Avallone, L.; Webster, C.; et al. Transport out of the lower stratospheric vortex by Rossby wave breaking. *J. Geophys. Res. Atmos.* **1994**, *99*, 1071–1088. [CrossRef]

40. Marchand, M.; Godin, S.; Hauchecorne, A.; Lefèvre, F.; Bekki, S.; Chipperfield, M.P. Influence of polar ozone loss on northern mid-latitude regions estimated by a high resolution chemistry transport model during winter 1999–2000. *J. Geophys. Res. Atmos.* **2003**, *108*, 8326. [CrossRef]
41. Shepherd, T.G. Transport in the Middle Atmosphere. *J. Meteorol. Soc. Jpn.* **2007**, *85B*, 165–191. [CrossRef]
42. Koch, G.; Wernli, H.; Staehelin, J.; Peter, T. A Lagrangian analysis of stratospheric ozone variability and long-term trends above Payerne (Switzerland) during 1970–2001. *J. Geophys. Res. Atmos. Atmos.* **2002**, *107*, ACL 2-1–ACL 2-14. [CrossRef]
43. Prather, M.; Jaffe, H. Global impact of the Antarctic ozone hole: Chemical propagation. *J. Geophys. Res. Atmos.* **1990**, *95*, 3413–3492. [CrossRef]
44. Waugh, D.W. Subtropical stratospheric mixing linked to disturbances in the polar vortices. *Nature* **1993**, *365*, 535–537. [CrossRef]
45. Manney, G.L.; Zurek, R.W.; Neil, A.O.; Swinbank, R. On the motion of air through the stratospheric polar vortex. *J. Atmos. Sci.* **1994**, *51*, 2973–2994. [CrossRef]
46. Reid, S.J.; Vaughan, G. Lamination in ozone profiles in the lower stratosphere. *Q. J. R. Meteorol. Soc.* **1991**, *117*, 825–844. [CrossRef]
47. Perez, A.; Crino, E.; De Carcer, I.A.; Jaque, F. Low-ozone events and three-dimensional transport at midlatitudes of South America during springs of 1996 and 1997. *J. Geophys. Res. Atmos.* **2000**, *105*, 4553–4561. [CrossRef]
48. Semane, N.; Bencherif, H.; Morel, B.; Hauchecorne, A.; Diab, R.D. An unusual stratospheric ozone decrease in Southern Hemisphere subtropics linked to isentropic air-mass transport as observed over Irene (25.5° S, 28.1° E) in mid-May 2002. *Atmos. Chem. Phys.* **2006**, *6*, 1927–1936. [CrossRef]
49. Brinksma, E.J.; Meijer, Y.J.; Connor, B.J.; Manney, G.L.; Bergwerff, J.B.; Bodeker, G.E.; Boyd, I.S.; Liley, J.B.; Hogervorst, W.; Hovenier, J.W.; et al. Analysis of record-low ozone values during the 1997 winter over Lauder, New Zealand. *Geophys. Res. Lett.* **1998**, *25*, 2785–2788. [CrossRef]
50. Orsolini, Y.J.; Manney, G.L.; Engel, A.; Ovarlez, J.; Claud, C.; Coy, L. Layering in stratospheric profiles of long-lived trace species: Balloonborne observations and modeling. *J. Geophys. Res. Atmos.* **1998**, *103*, 5815–5825. [CrossRef]
51. Hall, T.M.; Waugh, D.W. Tracer transport in the tropical stratosphere due to vertical diffusion and horizontal mixing. *Geophys. Res. Lett.* **1997**, *24*, 1383–1386. [CrossRef]
52. Heese, B.; Godin, S.; Hauchecorne, A. Forecast and simulation of stratospheric ozone filaments: A validation of a high-resolution potential vorticity advection model by airborne ozone lidar measurements in winter 1998/1999. *J. Geophys. Res. Atmos.* **2001**, *106*, 20011–20024. [CrossRef]
53. Portafaix, T.; Morel, B.; Bencherif, H.; Baldy, S.; Godin-Beekmann, S.; Hauchecorne, A. Fine-scale study of a thick stratospheric ozone lamina at the edge of the southern subtropical barrier. *J. Geophys. Res. Atmos.* **2003**, *108*, 4196. [CrossRef]
54. Hauchecorne, A.; Godin, S.; Marchand, M.; Heese, B.; Souprayen, C. Quantification of the transport of chemical constituents from the polar vortex to midlatitudes in the lower stratosphere using the high-resolution advection model MIMOSA and effective diffusivity. *J. Geophys. Res. Atmos.* **2002**, *107*, 8289. [CrossRef]
55. McIntyre, M.E.; Palmer, T.N. The "surf zone" in the stratosphere. *J. Atmos. Terr. Phys.* **1984**, *46*, 825–849. [CrossRef]
56. Kanzawa, H. Four observed sudden stratospheric warmings diagnosed by the Eliassen-Palm flux and refractive index. In *Dynamics of the Middle Atmosphere*; Holton, J.R., Matsuno, T., Eds.; Terra Sci.: Tokyo, Japan, 1984; pp. 307–331.
57. Morel, B.; Bencherif, H.; Keckhut, P.; Portafaix, T.; Hauchecorne, A.; Baldy, S. Fine-scale study of a thick stratospheric ozone lamina at the edge of the southern subtropical barrier: 2. Numerical simulations with coupled dynamics models. *J. Geophys. Res. Atmos.* **2005**, *110*, D17101. [CrossRef]
58. Bencherif, H.; El Amraoui, L.; Kirgis, G.; De Bellevue, J.L.; Hauchecorne, A.; Mzé, N.; Portafaix, T.; Pazmino, A.; Goutail, F. Analysis of a rapid increase of stratospheric ozone during late austral summer 2008 over Kerguelen (49.4°S, 70.3°E). *Atmos. Chem. Phys.* **2011**, *11*, 363–373. [CrossRef]
59. Kirchhoff, V.W.J.H.; Schuch, N.J.; Pinheiro, D.K.; Harris, J.M. Evidence for an ozone hole perturbation at 30° south. *Atmos. Environ.* **1996**, *33*, 1481–1488. [CrossRef]
60. Guarnieri, R.A.; Padilha, L.F.; Guarnieri, F.L.; Echer, E.; Makita, K.; Pinheiro, D.K.; Schuch, A.M.P.; Boeira, L.S.; Schuch, N.J. A study of the anticorrelations between ozone and UV-B radiation using linear and exponential fits in southern Brazil. *Adv. Space Res.* **2004**, *34*, 764–768. [CrossRef]
61. Schuch, P.A.; Santos, M.B.; Lipinski, V.M.; Peres, L.V.; Santos, C.P.; Cechin, S.Z.; Schuch, N.J.; Pinheiro, D.K.; Loreto, E.L.S. Identification of influential events concerning the Antarctic ozone hole over southern Brazil and the biological effects induced by UVB and UVA radiation in an endemic tree frog species. *Ecotoxicol. Environ. Saf.* **2015**, *118*, 190–198. [CrossRef]
62. Peres, L.V.; Bencherif, H.; Mbatha, N.; Schuch, A.P.; Toihir, A.M.; Bègue, N.; Portafaix, T.; Anabor, V.; Pinheiro, D.K.; Leme, N.M.P.; et al. Measurements of the total ozone column using a Brewer spectrophotometer and TOMS and OMI satellite instruments over the Southern Space Observatory in Brazil. *Ann. Geophys.* **2017**, *35*, 25–37. [CrossRef]
63. Chiodo, G.; Polvani, L.M. The response of the ozone layer to quadrupled CO_2 concentrations: Implications for climate. *J. Clim.* **2019**, *32*, 7629–7642. [CrossRef] [PubMed]
64. Chiodo, G.; Polvani, L.M.; Marsh, D.R.; Stenke, A.; Ball, W.; Rozanov, E.; Muthers, S.; Tsigaridis, K. The response of the ozone layer to quadrupled CO_2 concentrations. *J. Clim.* **2018**, *31*, 3893–3907. [CrossRef]
65. Bresciani, C.; Bittencourt, G.D.; Bageston, J.V.; Pinheiro, D.K.; Schuch, N.J.; Bencherif, H.; Leme, N.P.; Peres, L.V. Report of a large depletion in the ozone layer over southern Brazil and Uruguay by using multi-instrumental data. *Ann. Geophys.* **2018**, *36*, 405–413. [CrossRef]

66. Bittencourt, G.D.; Bresciani, C.; Pinheiro, D.K.; Bageston, J.V.; Schuch, N.J.; Bencherif, H.; Leme, N.P.; Peres, L.V. A major event of Antarctic ozone hole influence in southern Brazil in October 2016: An analysis of tropospheric and stratospheric dynamics. *Ann. Geophys.* **2018**, *36*, 415–424. [CrossRef]
67. Peres, L.V.; Pinheiro, D.K.; Steffenel, L.A.; Mendes, D.; Bageston, J.V.; Bittencourt, G.D.; Schuch, A.P.; Anabor, V.; Leme, N.M.P.; Schuch, N.J.; et al. Long term monitoring and climatology of stratospheric fields when the occurrence of influence of the antarctic ozone hole over south of Brazil events. *Rev. Bras. Meteorol.* **2019**, *34*, 151–163. [CrossRef]
68. Rasera, G.; Anabor, V.; Steffenel, L.A.; Pinheiro, D.K.; Puhales, F.S.; Rodrigues, L.G.; Peres, L.V. Analysis of significant stratospheric ozone reductions over southern Brazil: A proposal for a diagnostic index for southern South America. *Meteorol. Appl.* **2021**, *28*, e2034. Available online: https://rmets.onlinelibrary.wiley.com/doi/full/10.1002/met.2034 (accessed on 25 February 2023). [CrossRef]
69. Kerr, J.B.; McElroy, C.T.; Wardle, D.I.; Olafson, R.A.; Evans, W.F. The automated Brewer Spectrophotometer, Proceed. In Proceedings of the Quadrennial Ozone Symposium, Halkidiki, Greece, 3–7 September 1984; Zerefos, C.S., Ghazi, A., Eds.; D. Reidel: Norwell, MA, USA, 1985; pp. 396–401.
70. Kerr, J.B. New methodology for deriving total ozone and other atmospheric variables from Brewer spectrometer direct Sun spectra. *J. Geophys. Res. Atmos.* **2002**, *107*, 4731. [CrossRef]
71. Schuch, N.J.; Costa, J.M.; Kirchhoff, V.W.J.H.; Dutra, S.G.; Sobral, J.H.A.; Abdu, M.A.; Takahashi, H.; Adaime, S.F.; Oliveira, N.U.V.; Bortolotto, E.; et al. O Observatório Espacial do Sul: Centro Regional do Sul de Pesquisas Espaciais OES/CRSPE/INPE em São Martinho da Serra—RS. *Rev. Bras. Geofísica* **1997**, *15*. [CrossRef]
72. McPeters, R.D.; Bhartia, P.K.; Krueger, A.J.; Herman, J.R.; Wellemeyer, C.G.; Seflor, G.; Jaross, C.F.; Torres, O.; Moy, L.; Abow, G.; et al. *Earth Probe Total Ozone Mapping Spectrometer (TOMS) Data Products User Guide*; Tech. Rep. TP-1998-206895; NASA: Washington, DC, USA, 1998.
73. Antón, M.; López, M.; Vilaplana, J.M.; Kroon, M.; McPeters, R.; Bañón, M.; Serrano, A. Validation of OMI-TOMS and OMI-DOAS total ozone column using five Brewer spectroradiometers at the Iberian Peninsula. *J. Geophys. Res. Atmos.* **2009**, *114*, D14307. [CrossRef]
74. Waters, J.W.; Froidevaux, L.; Harwood, R.S.; Jarnot, R.F.; Pickett, H.M.; Read, W.G.; Siegel, P.H.; Cofield, R.E.; Filipiak, M.J.; Flower, D.A.; et al. The Earth Observing System Microwave Limb Sounder (EOS MLS) on the Aura Satellite. *IEEE Trans. Geosci. Remote* **2006**, *44*, 1075–1092. [CrossRef]
75. Livesey, N.J.; Santee, M.L.; Manney, G.L. A Match-based approach to the estimation of polar stratospheric ozone loss using Aura Microwave Limb Sounder observations. *Atmos. Chem. Phys.* **2015**, *15*, 9945–9963. [CrossRef]
76. Godin, S.; Marchand, M.; Hauchecorne, A. Influence of the Arctic polar vortex erosion on the lower stratospheric ozone amount at Haute-Provence Observatory (43.92°N, 5.71°E). *J. Geophys. Res. Atmos.* **2002**, *107*, 8272. [CrossRef]
77. Bencherif, H.; Diab, R.D.; Portafaix, T.; Morel, B.; Keckhut, P.; Moorgawa, A. Temperature climatology and trend estimates in the UTLS region as observed over a southern subtropical site, Durban, South Africa. *Atmos. Chem. Phys.* **2006**, *6*, 5121–5128. [CrossRef]
78. Holton, J.R.; Haynes, P.H.; Mcintyre, M.E.; Douglass, A.R.; Rood, R.B.; Pfister, L. Stratosphere-troposphere Exchange. *Rev. Geophys.* **1995**, *3*, 403–439. [CrossRef]
79. Nakamura, N. Two-dimensional mixing, edge formation, and permeability diagnosed in an area coordinate. *J. Atmos. Sci.* **1996**, *53*, 1524–1537. [CrossRef]
80. Thompson, A.M.; Witte, J.C.; McPeters, R.D.; Oltmans, S.J.; Schmidlin, F.J.; Logan, J.A.; Fujiwara, M.; Kirchhoff, V.W.J.H.; Posny, F.; Coetzee, G.J.R.; et al. Southern Hemisphere Additional Ozonesondes (SHADOZ) 1998–2000 tropical ozone climatology 1. Comparison with Total Ozone Mapping Spectrometer (TOMS) and ground-based measurements. *J. Geophys. Res. Atmos.* **2003**, *108*, 8238. [CrossRef]
81. Wilks, S.D. *Statistical Methods in the Atmospheric Sciences, an Introduction*; Academic Press: San Diego, CA, USA, 1995; p. 464.
82. Hendrick, F.; Pommereau, J.-P.; Goutail, F.; Evans, R.D.; Ionov, D.; Pazmino, A.; Kyrö, E.; Held, G.; Eriksen, P.; Dorokhov, V.; et al. NDACC/SAOZUV-visible total ozone measurements: Improved retrieval and comparison with correlative ground-based and satellite observations. *Atmos. Chem. Phys.* **2011**, *11*, 5975–5995. [CrossRef]
83. Nakamura, N. A new look at eddy diffusivity as a mixing diagnostic. *J. Atmos. Sci.* **2001**, *58*, 3685–3701. [CrossRef]
84. Mariotti, A.; Moustaoui, M.; Legras, B.; Teitelbaum, H. Comparison between vertical ozone soundings and reconstructed potential vorticity maps by contour advection with surgery. *J. Geophys. Res. Atmos.* **1997**, *102*, 6131–6142. [CrossRef]
85. Orsolini, Y.J.; Grant, W.B. Seasonal formation of nitrous oxide laminae in the mid and low latitude stratosphere. *Geophys. Res. Lett.* **2000**, *27*, 1119–1122. [CrossRef]
86. Randel, W.J.; Gille, J.C.; Roche, A.E.; Kumer, J.B.; Mergenthaler, J.L.; Waters, J.W.; Fishbein, E.F.; Lahoz, W.A. Stratospheric transport from the tropics to middle latitudes by planetary-wave mixing. *Nature* **1993**, *365*, 533–537. [CrossRef]
87. Toihir, A.M.; Sivakumar, V.; Bencherif, H.; Portafaix, T. Study on variability and trend of Total Column Ozone (TCO) obtained from combined satellite (TOMS and OMI) measurements over the southern subtropic. In Proceedings of the 30th Annual Conference of South African Society for Atmosphere Science, Potchefstroom, South Africa, 1–2 October 2014; pp. 109–112.
88. Toihir, A.M.; Portafaix, T.; Sivakumar, V.; Bencherif, H.; Pazmiño, A.; Bègue, N. Variability ad trend in ozone over the southern tropics and subtropics. *Ann. Geophys.* **2018**, *36*, 381–404. [CrossRef]

89. Toihir, A.M.; Bencherif, H.; Sivakumar, V.; El Amraoui, L.; Portafaix, T.; Mbatha, N. Comparison of total column ozone obtained by the IASI-MetOp satellite with ground-based and OMI satellite observations in the southern tropics and subtropics. *Ann. Geophys.* **2015**, *33*, 1135–1146. [CrossRef]
90. Steffenel, L.A.; Anabor, V.; Pinheiro, D.K.; Guzman, L.; Bittencourt, G.D.; Bencherif, H. Forecasting upper atmospheric scalars advection using deep learning: An O_3 experiment. *Mach. Learn.* **2021**, *112*, 765–788. [CrossRef]
91. Guzmán, L.; Anabor, V.; Steffenel, L.A.; Pinheiro, D.K. Numerical and observational study of an event of decrease in the total ozone column of tropical origin in Southern Brazil. *Ciência E Nat.* **2020**, *42*, e5. [CrossRef]
92. Bittencourt, G.D.; Pinheiro, D.K.; Bageston, J.V.; Bencherif, H.; Steffenel, L.A.; Vaz Peres, L. Investigation of the behavior of the atmospheric dynamics during occurrences of the ozone hole's secondary effect in southern Brazil. *Ann. Geophys.* **2019**, *37*, 1049–1061. [CrossRef]
93. Souza, A.M.; Peres, L.V.; Bittencourt, G.D.; Pinheiro, D.K.; Lopes, B.C.; Anabor, V.; Leme, N.M.; Martins, M.P.P.; DA Silva, R.; DOS Reis, G.C.; et al. Impacts of the Antartic ozone hole influence events over southern Brazil in October 2015. *An. Da Acad. Bras. De Ciências* **2023**, *95* (Suppl. 3), e20210528. [CrossRef]